Hindawi
Advances in Civil Engineering
Volume 2020, Article ID 6365354, 16 pages
https://doi.org/10.1155/2020/6365354

Research Article

An Experimental Study of the Feasibility of Identifying the Impact Damages of Reinforced Concrete Piers Using a Modal Frequency Method

Xiwu Zhou, Wenchao Zhang, Yushen Gao, Guoxue Zhang, and Mengdan Wen

School of Transportation and Civil Engineering and Architecture, Foshan University, Foshan, China

Correspondence should be addressed to Wenchao Zhang; 1350392000@qq.com

Received 14 June 2019; Revised 7 November 2019; Accepted 28 December 2019; Published 22 January 2020

Academic Editor: Giovanni Garcea

In this research study, horizontal impact tests were carried out on five reduced scale pier models using China's most advanced multifunctional ultrahigh heavy drop hammer impact test system and DHDAS dynamic signal acquisition and analysis system. Due to the fact that the traditional measurement method can only be used for local measurement damage, and the volatility is high, this paper proposes a test method for the modal frequency identification of the overall damage of reinforced concrete pier and applies the ultrasonic damage measurement method to verify the results. The tests analyzed the modal frequencies and ultrasonic velocity identifications for the purpose of evaluating the impact damages of bridge piers, as well as the relationship between them. The results showed that the modal frequencies were consistent with the ultrasonic waves in identifying and evaluating the damages to the piers. Also, the modal frequency damage factors were determined to be functions of the ultrasonic wave velocity damage factors. Therefore, the results of this study confirmed that it was feasible to characterize the impact damages of piers using a modal frequency method.

1. Introduction

Pier structures may become damaged, cracked, or aged to varying degrees for a variety of reasons during their utilization. With China's recent economic and infrastructure development, many types of river-crossing and sea-crossing bridges have been rapidly developed, which have resulted in ship-bridge collision accidents occurring more frequently. Therefore, in order to ensure the safety and durability of pier structures, it is of great significance to examine the impact damages of reinforced concrete piers [1–3].

In recent years, researchers around the world have carried out studies regarding the identification of RC structural damages and have proposed a variety of identification methods [4–6]. These methods mainly include static, dynamic, and dynamic-static combination methods. The static method is to analyze the static test data (force and displacement) to determine the change of structural element stiffness, which can then be used for damage assessments and the determination of structural bearing capacities [7]. Dynamic identification methods mainly use vibration modes, transfer functions, curvature modes, frequency response functions, and relative acceleration to identify damage [8–10]. Dynamic-static combination methods seek to identify structural damage by using the static deflection, vibration mode, and output error method [11,12]. At present, the most commonly used damage identification methods are traditional experimental methods, such as acoustic or ultrasonic methods, electromagnetic methods, and radiography methods [13–15]. These methods require the damage areas to be known beforehand, and it must be easy for the damage detection sensor to reach the tested part. In addition, these sensors are only able to detect small areas of the structural or adjacent surfaces. Therefore, these methods have very limited application potential. It is known that different types of structures have different damage forms. In regard to reinforced concrete piers, the main damages which occur are the results of impacts with ships and vehicles [16–19]. At the present time, the research studies regarding the impact damages of reinforced concrete piers

have mainly been based on traditional experimental and numerical simulation methods. For example, Zhang and Zhou et al. applied ultrasonic detectors to identify the damages of concrete piers and evaluate the damage of piers based on the change of ultrasonic wave velocity [20, 21]. Gholipour and Ren et al. used the numerical simulation method to identify the damages of concrete piers [22, 23]. Some researchers have also performed identifications of pier impact damages using modal parameters. For example, Zhan et al. proposed an impact vibration test method for measuring the natural frequencies of existing piers and carried out numerical research examinations [24, 25]. The previous studies conducted by Yuen and Pandey et al. showed that the vibration mode ratio, characteristic parameters, and curvature modal difference indexes could be directly obtained from the measured frequencies and modes. This information could then be directly used for damage identifications without requiring finite element models of the target structures. Therefore, this method possessed the characteristics of a model-free indexing method [26, 27]. You-Sheng completed a comparative analysis of several calculation methods for the natural frequencies of pile foundation piers and pointed out their respective advantages and disadvantages [28]. However, these studies mainly use impact vibration test methods and numerical research methods.

Currently, the most commonly accepted and promising damage identification method is a cross-disciplinary experimental modal analysis method. This method combines system identification, vibration theory, vibration testing technology, signal acquisition, and analysis. It has been found that the results of identifications of structural damages using modal frequencies to assess the overall damages of structures and study the overall damage information of the structures have shown high antinoise and identification accuracy abilities. Also, these types of methods have been observed to have convenient measurement adaptabilities [29–31]. Furthermore, this method has been widely used in aviation, aerospace, precision machine tools, and other fields in developed countries, for fault diagnosis, load identification, and dynamic modification. However, the applications of this method for pier impact damage detections have seldom been reported. Therefore, this study proposed to use a modal frequency method to identify the impact damages of reinforced concrete piers. A multifunctional ultrahigh heavy drop hammer impact test system and a DHDAS dynamic signal acquisition and analysis system were utilized in this study to carry out experimental horizontal impact tests on five reduced scale pier model specimens. The feasibility and accuracy of identification in the evaluations of the pier impact damages using modal frequencies were examined and analyzed, and a traditional ultrasonic velocity method was used for verification purposes.

2. Experimental Impact Tests

2.1. Test Equipment

2.1.1. Horizontal Impact Equipment. This study's impact tests adopted a multifunctional ultrahigh heavy drop hammer testing machine system, which consisted of a vertical drop hammer driving system and a horizontal impact system. The experimental equipment was able to obtain vertical and horizontal two-way impact data, as shown in Figure 1(a). The kinetic energy of the horizontal impact test cart (hereinafter referred to as the cart, as detailed in Figure 1(b)) was provided by the vertical drop hammer driving system (Figure 1(c)). The dimensions of the car were $L \times W \times H = 2.08\,\text{m} \times 1.15\,\text{m} \times 0.64\,\text{m}$. The front end of the cart was equipped with a rigid impact hammer measuring $L \times B = 590\,\text{mm} \times 220\,\text{mm}$. There were four specially designed steel cylinder installation pressure sensors located between the hammer and the cart. At the end of the track, a laser velocity measurement system was used to measure the instantaneous speeds of the impacts, as shown in Figure 1(d).

The impact velocity (kinetic energy) of the cart was related to the lifting height and mass of the drop hammer, as well as the mass of the cart. Among these, the maximum lifting height of the hammer was 18 m; the mass of the hammer was 166 kg; and the mass of the cart was $m_1 = 1{,}200$ kg. The mass totals of the drop hammer and cart could be adjusted using weight blocks.

2.1.2. Modal Frequency Acquisition Equipment. During the modal analysis, an example of the cohesive hammer used is shown in Figure 2(a). A DHDAS (Dong-Hua Test Real Time Data Measurement and Analysis Software System) dynamic signal acquisition and analysis system (Figure 2(b)) was adopted for the acquisition of the excitation signals, and the pier response signals were measured using an acceleration sensor (Figure 2(c)). Then, a spectral analysis was conducted on the measured signals in order to obtain the transfer functions, implement the fitting of the transfer functions, and determine the natural frequencies of the piers in combination with the vibration mode. The whole test system is shown in Figure 3.

2.1.3. Ultrasonic Wave Velocity Acquisition Equipment. The concrete damage of the main damaged area of the test piece was detected by a ZBL-U520 nonmetal ultrasonic detector (as shown in Figure 4). In the test, the measuring points in the high damage area such as the impact point area and the bottom area of the test piece were examined.

2.2. Test Specimens. Five reinforced concrete circular pier specimens were designed for this study's experimental tests. The column section radius of each specimen was 170 mm, and the height of each specimen was 2,200 mm. The selected stirrup was I-grade ordinary steel bar HPB300 with a diameter of 8 mm, which adopted a welding construction. The model is shown in Figure 5. The longitudinal reinforcements were HRB400 reinforcements. The pier model numbers and design parameters are shown in Table 1. The longitudinal reinforcements and distributions of the specimens are detailed in Figure 6.

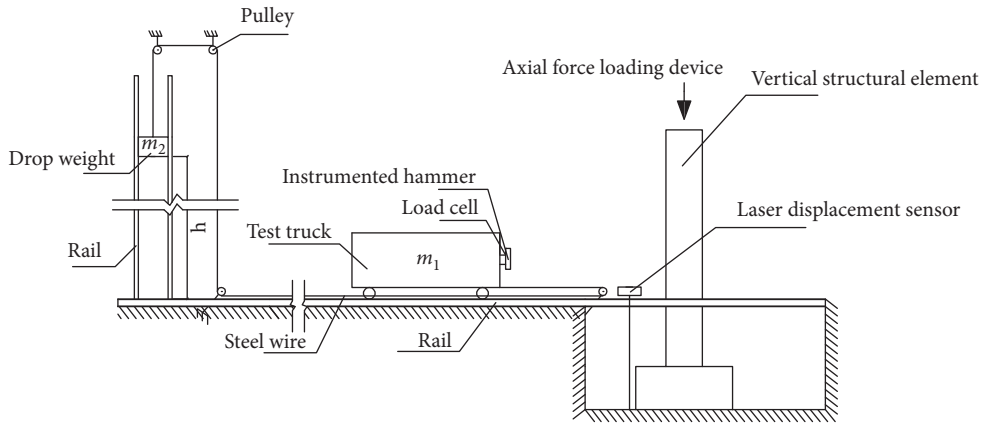

(a)

(b)

(c)

(d)

Figure 1: (a) Multifunctional ultrahigh heavy drop hammer testing machine system, (b) horizontal traction impact testing cart, (c) vertical drop hammer device, and (d) laser velocimetry.

(a)

(b)

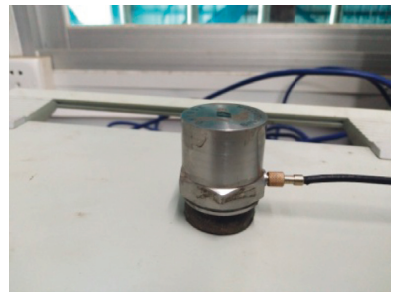

(c)

Figure 2: (a) Cohesive hammer; (b) DHDAS dynamic signal acquisition and analysis system; (c) acceleration sensor.

Reinforcement samples were taken from the specimens for the testing process. Also, loading-tension tests were carried out on an electrohydraulic servo universal testing machine, which obtained the yield strengths and ultimate strengths of the steel bars. At the same time, six test cubes (150 mm × 150 mm × 150 mm) were constructed according to requirements of the experiments, and compression tests were carried out on the specimens. The basic parameters of the steel bars and concrete are shown in Table 2.

2.3. Test Design. Horizontal impact tests were carried out on the five reinforced concrete column specimens. Each column

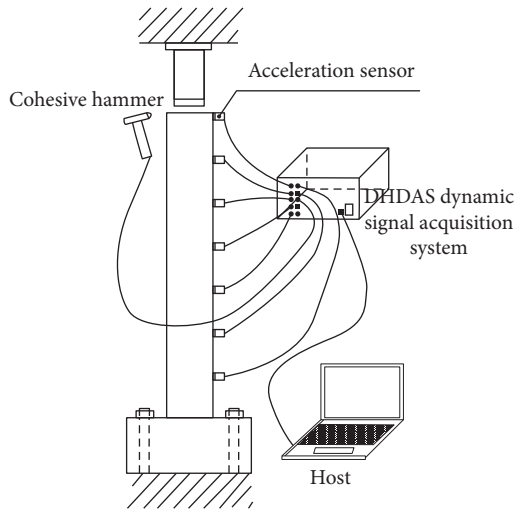

Figure 3: Modal test system.

(a) (b)

Figure 4: (a) ZBL-U520 host; (b) ultrasonic transmitter.

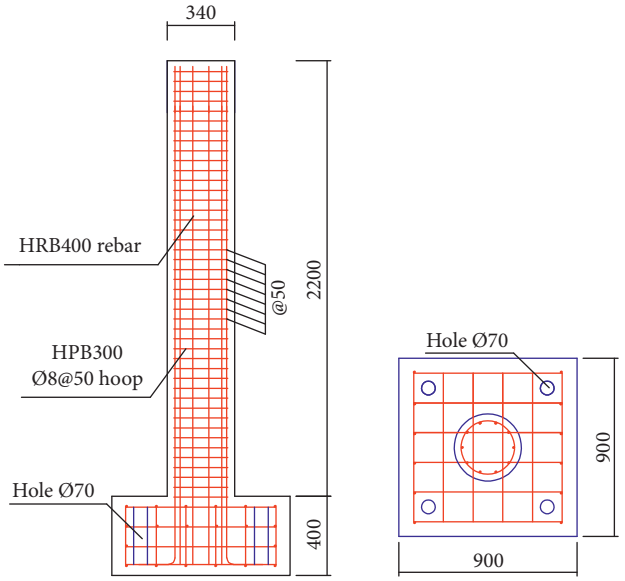

Figure 5: Schematic diagram of the specimens' reinforcements.

was planned to be impacted four times, in which the Z16-1 and Z20-1 specimens followed Scheme 1, while the Z16-2, Z16-3, and Z20-2 specimens adopted Scheme 2. The scheme details are shown in Tables 3 and 4. Then, based on the principle of the conservation of energy, the theoretical speeds of the impacts were calculated as follows:

$$m_2 gh = \frac{1}{2}(m_1 + m_2)v_1^2 + \mu m_1 gh, \quad (1)$$

where m_1 and m_2 denote the masses of the cart and drop hammer, respectively; $g = 9.81\ \mathrm{m/s^2}$ is the gravitational acceleration; h represents the drop height of the hammer before release; v_1 is the instantaneous velocity of the test cart before impact; and μ denotes the friction coefficient between the rail and the test cart, which was calibrated and determined by the preliminary impact test results, and for the different m_1 and h. The friction coefficient was approximately equaled to 0.12. A laser velocity measurement system was installed at the end of the track for the purpose of measuring the instantaneous velocities of the impacts. As detailed in Tables 3 and 4, the measured velocities were approximately equal to the theoretical velocities obtained using formula (1) (the rate of the velocity variation was ±5%), which verified the reliability and accuracy of the impact test system.

Prior to the testing, the pier specimens were fixed on rigid bases with four prestressed bolts, which were

Table 1: Test specimen numbers and design parameters.

Specimen no.	Longitudinal reinforcement (mm)	Stirrup (mm)	Concrete strength grade
Z16-1	10Φ16	Φ8@50	C40
Z16-2	10Φ16	Φ8@50	C40
Z16-3	10Φ16	Φ8@50	C40
Z20-1	10Φ20	Φ8@50	C40
Z20-2	10Φ20	Φ8@50	C40

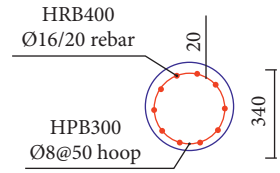

Figure 6: Longitudinal reinforcements and distributions of the specimens.

Table 2: Basic parameters of the steel bars and concrete.

Steel diameter	Elastic modulus of reinforcement (N/mm^2)	Yield strength (N/mm^2)	Ultimate strength (N/mm^2)	Elastic modulus of concrete (N/mm^2)	Concrete strength (N/mm^2)
Φ16	2.0×105	440	580	3.28×104	45.63
Φ20		486	640		

Table 3: Impact scheme 1.

Impact times	Drop height (m)	Car quality (kg)	Axial pressure (kN)	Drop hammer quality (kg)	Friction coefficient	Theoretical speed (m/s)	Measured average velocity (m/s)	Speed change rate (%)
1	4	1200	250	166	0.12	1.124	1.114	−0.890
2	6	1200	250	166	0.12	1.376	1.335	−2.980
3	8	1200	250	166	0.12	1.589	1.563	−1.636
4	10	1200	250	166	0.12	1.777	1.770	−0.56

Table 4: Impact scheme 2.

Specimen no.	Impact times	Drop height (m)	Car quality (kg)	Axial pressure (kN)	Drop hammer quality (kg)	Friction coefficient	Theoretical speed (m/s)	Measured average velocity (m/s)	Speed change rate (%)
Z16-2	4	6	1200	250	166	0.12	1.376	1.337	−2.834
Z16-3	4	8	1200	250	166	0.12	1.589	1.513	−4.783
Z20-2	4	8	1200	250	166	0.12	1.589	1.588	−0.0629

considered to be approximately equivalent to fixed end constraints. The upper ends of the columns were subjected to axial pressure of 250 kN by an oil jack mounted on the cross beam of the reaction frame, as shown in Figure 7. After installing each of the reinforced concrete column specimens, the drop hammer was raised to set heights to carry out the impact tests. For all of the tests, the impact points were located 1,100 mm from the bottom of each column, i.e., at the center of each specimen.

Seven acceleration sensors were evenly arranged on the back of each specimen during the tests (as shown in Figure 8). Prior to and following each impact, a cohesive hammer was used to impact the top of the impact surface of each specimen. At the same time, a DHDAS dynamic signal acquisition and analysis system was used to collect the excitation signals and pier response signals measured by the acceleration sensors for the purpose of obtaining the natural vibration frequencies of the pier specimens and carry out damage identification processes of the concrete piers. A ZBL-U520 nonmetallic ultrasonic testing instrument was used to detect the damages to the concrete pier specimens in the main damage areas. In this way, the feasibility and accuracy of identifications and evaluations of the pier impact damages using modal frequencies were successfully verified.

3. Feasibility Analysis of Modal Frequency Identification of Pier Damage

3.1. Modal Frequency Acquisition of Pier. After the modal test method was used to obtain the pier response signal, the

Figure 7: Axial pressure device.

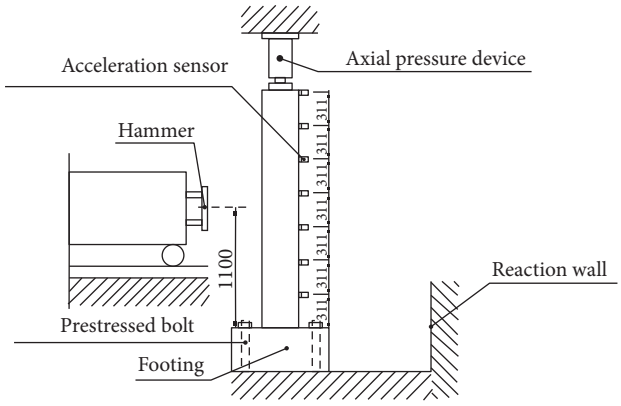

Figure 8: Arrangements of the restraint device and acceleration sensors.

DHDAS dynamic signal acquisition and analysis system was applied for data analysis (specimen Z16-1 was selected as an example). This system mainly included the model building, data import, parameter identification, mode shape determination, and modal verification.

3.1.1. Model Building. An analytical model corresponding to the distribution of the test pier and acceleration sensor was established (as shown in Figure 9).

3.1.2. Data Import. When importing data, the measurement method selects the "measurement method," and the method selects single-point excitation. The frequency response function is used to analyze the data (as shown in Figure 10).

3.1.3. Parameter Identification. The parameter identification method applied in this experiment uses the internationally

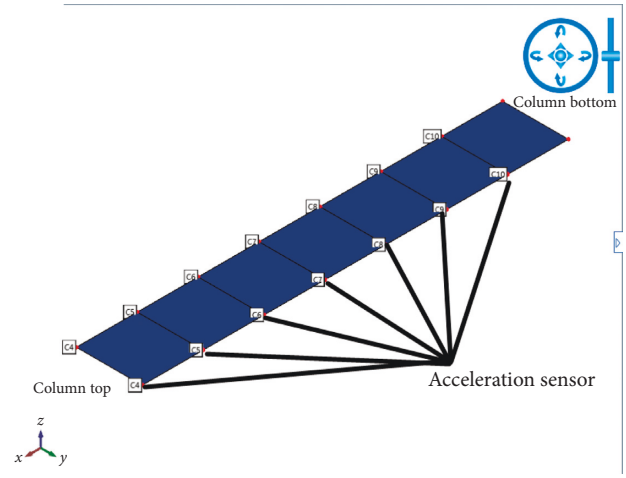

Figure 9: Analysis model.

emerging transfer function-based Polylscf, which is able to obtain a very clear steady-state graph, and the recognition accuracy of each modal parameter is very high. The method mainly includes three parts: frequency band selection, steady-state graph calculation, and frequency response curve fitting.

(1) Frequency band selection: the vertical cursor on the left side is typically placed at the far left when the band is selected. When moving the horizontal cursor to determine the number of nodes, in most cases the number of nodes should be greater than 3. After determining the frequency range and the number of nodes, the steady-state graph calculation can be performed (as shown in Figure 11).

(2) Steady-state graph calculation: in the calculation of the steady-state graph, the letter *S* indicates that all three modal parameters have reached a steady state, while *V* indicates that only the frequency and modal participation factors have been stabilized. We then select the pole corresponding to the frequency point of *S* to perform the vibration mode calculation. For the normalization method, the maximum value of the mode shape is selected to be normalized, after which the calculation of the modal parameters can be completed (as shown in Figure 12).

(3) Frequency response curve fitting: after the modal parameter calculation has been completed, the effect of fitting the frequency response curve of each measuring point can then be viewed, and the fitting degree shown in Figure 13 is 0.94.

3.1.4. Mode Shape Determination. After the modal parameters have been calculated, the modal shapes of each stage can be viewed in the mode animation display interface. As the test column of this paper is equivalent to the cantilever beam, the accuracy of the mode shape in the test can then be verified through comparison with the theoretical

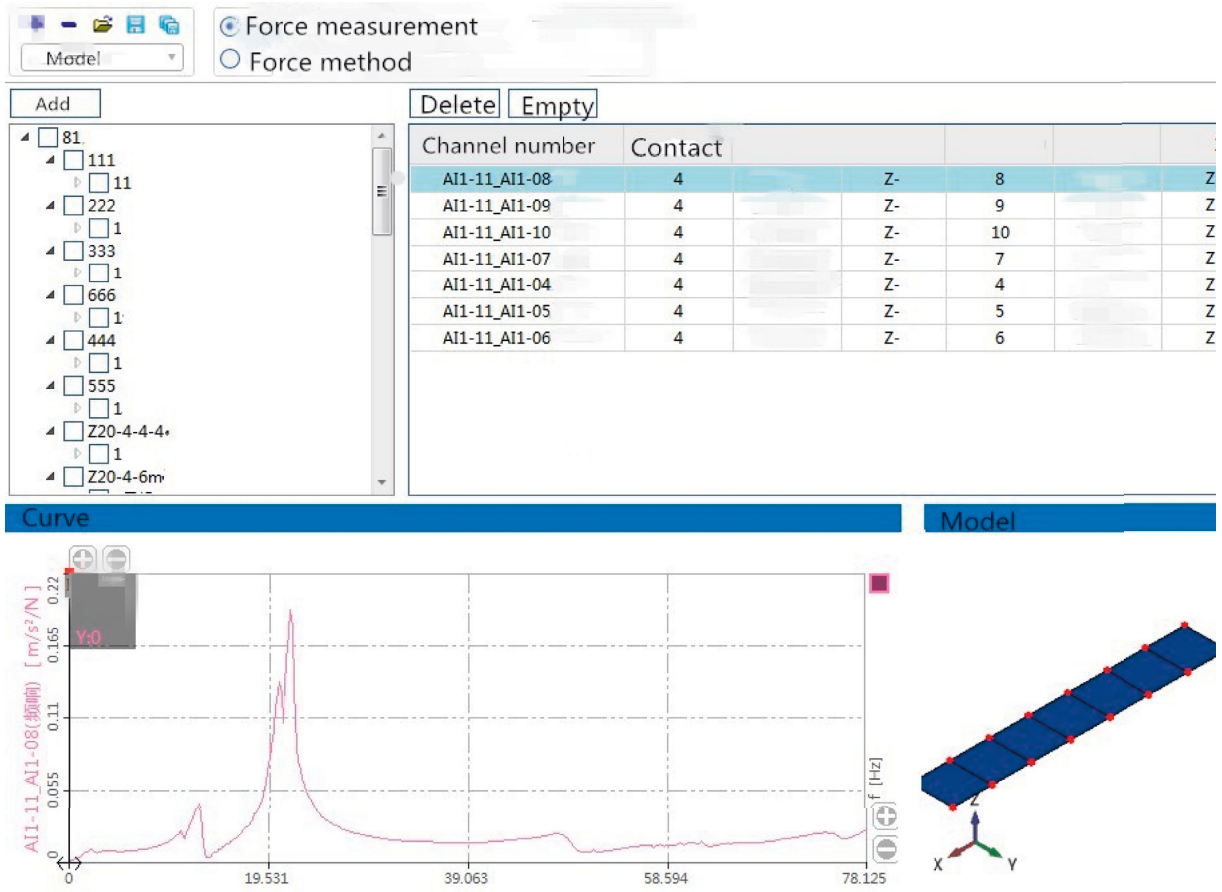

Figure 10: Force measurement data import.

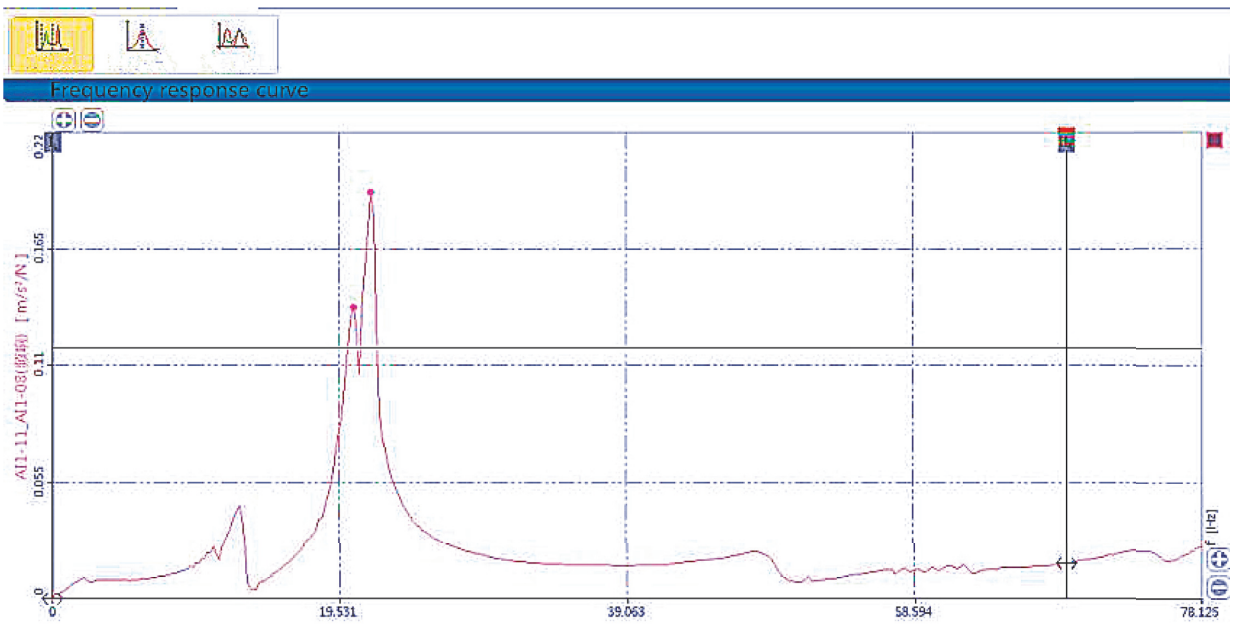

Figure 11: Frequency band selection.

mode shape of the cantilever beam (as shown in Figure 14). If the theoretical mode shape has not been met, then the test is repeated.

3.1.5. Modal Verification. The verification results of each modal parameter file, mainly MAC, MSF, and MOV, are viewed. This modal verification is as follows.

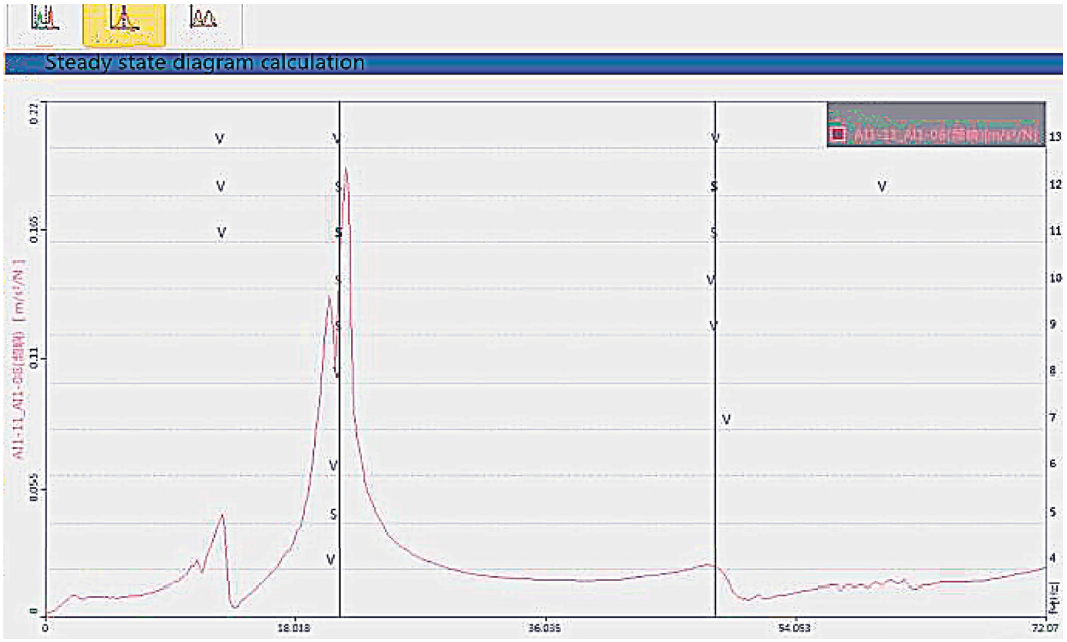

Figure 12: Steady-state graph calculation.

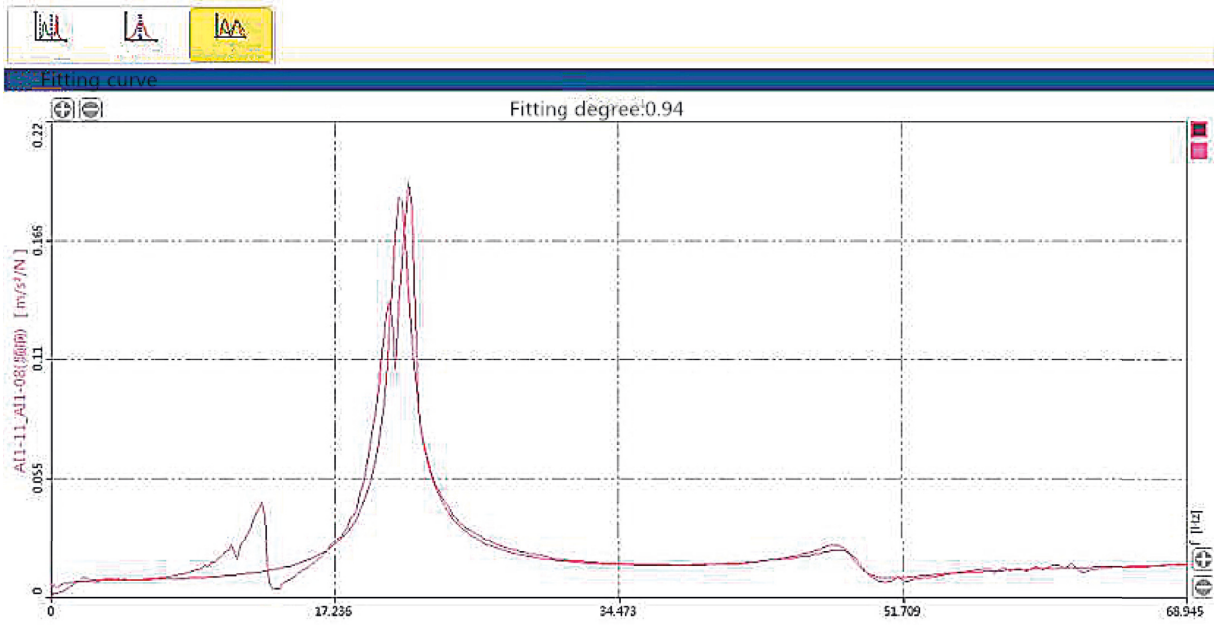

Figure 13: Frequency response curve fitting.

Figure 15 shows a schematic diagram for the distribution of the modal assurance criterion (MAC) and modal scale factor (MSF) array. As can be seen in the diagram, the majority of the modal analysis results were found to be ideal, with low modal influence and good decoupling observed. Among the three modal validation parameters detailed in Table 5, the MAC, MSF, and MOV (modal complexity) of the first modal frequency were all 1. These results indicated that the first modal frequency obtained from the test was the true physical modal frequency of the pier.

3.2. Experimental Modal Frequency to Identify Pier Damage. The first-order modal frequencies of five test pier models before and after impact are obtained by the abovementioned modal frequency acquisition and analysis method. The modal frequency is a function of pier stiffness. Therefore, when the pier is damaged, the modal frequency will change correspondingly. In this study, by analyzing the changes in the modal frequencies, the positions and degrees of the damages could be determined. It is known that the pier stiffness will change after damages occur. In this study, the

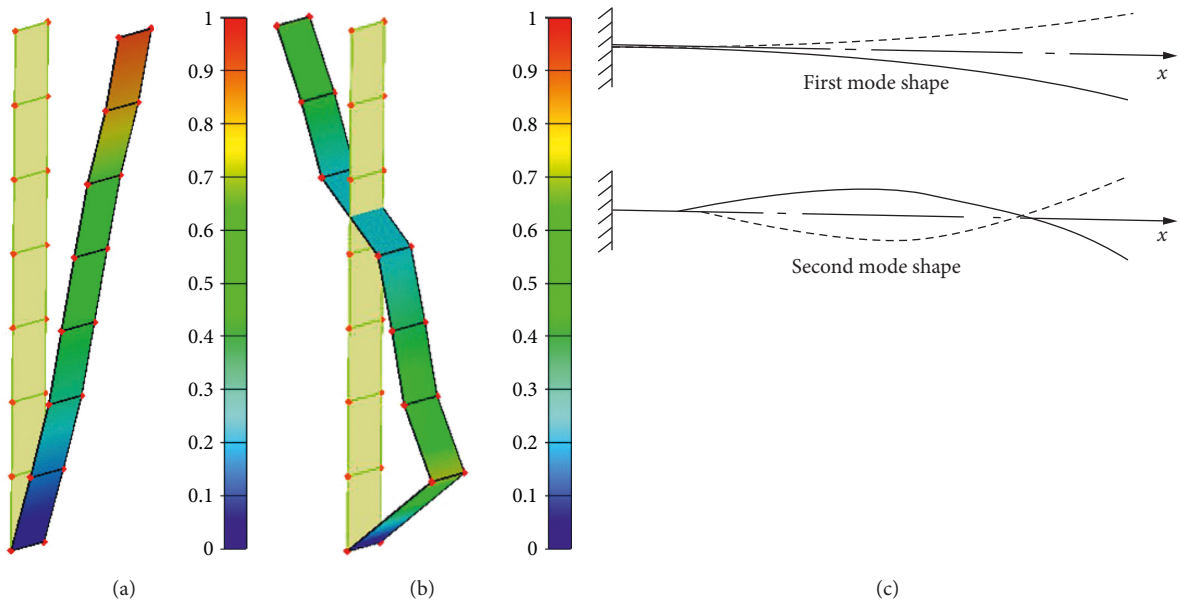

Figure 14: (a) First mode shape; (b) second mode shape; (c) theoretical mode shape of the cantilever beam.

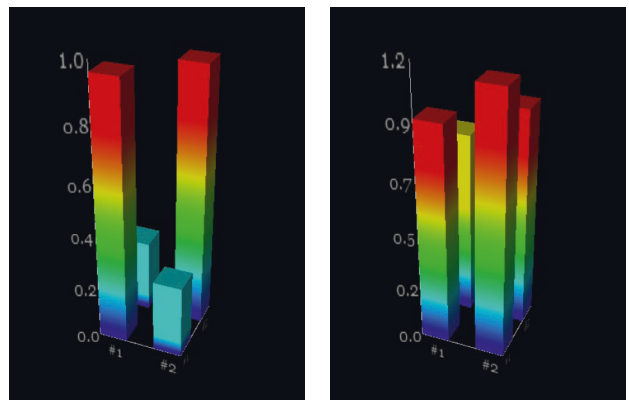

Figure 15: (a) Modal assurance criterion (MAC); (b) modal scale factor (MSF).

Table 5: Parameters relating to the modal verifications.

Serial number	Frequency	MAC		MSF		MOV
		First order	Second order	First order	Second order	
First order	27.34	1.00	0.29	1.00	1.18	1.00
Second order	56.66	0.29	1.00	0.85	1.00	0.25

change rates of component stiffness were adopted to represent the pier damages, and the damage factor D_1 of pier damage was defined for the first time in this research study as follows:

$$D_1 = \frac{\Delta K}{K} = 1 - \frac{\omega_b^2}{\omega_0^2}, \quad (2)$$

where ω_0 is the frequency (Hz) before damage and ω_b is the frequency (Hz) after damage.

The experimentally measured data and the calculated D_1 are shown in the following table:

It can be seen from Table 6 that, with the increase of impact times, the first-order modal frequency gradually decreases, the damage factor gradually increases, and the change trend of modal frequency and damage factor remains consistent. This is due to the fact that the pier is gradually damaged with the increase of impact times, and the rigidity decreases. Therefore, the damage factor characterized by the

Table 6: Identification of the pier damages using the modal frequencies of the test columns.

Specimen no.	Impact time	Impact velocity (m/s)	Impact energy (J)	First-order frequency (Hz)		Damage factor D_1
				Before impact ω_0	After impact ω_b	
Z16-1	1	1.181	836.8566	27.337	23.538	0.258626
	2	1.376	1136.026	23.538	22.78	0.305606
	3	1.589	1514.953	22.78	21.194	0.398931
	4	1.717	1768.853	21.194	19.7	0.480685
Z20-1	1	1.047	657.7254	23.116	21.242	0.207939
	2	1.354	1099.99	21.242	21.017	0.224629
	3	1.603	1541.765	21.017	20.985	0.226989
	4	1.806	1956.982	20.985	19.544	0.329506
Z16-2	1	1.378	1139.33	24.365	20.453	0.219390
	2	1.336	1070.938	20.453	20.062	0.295337
	3	1.316	1039.114	20.062	19.271	0.322022
	4	1.316	1039.114	19.271	18.565	0.374430
Z16-3	1	1.496	1342.81	22.817	19.362	0.279916
	2	1.496	1342.81	19.362	19.118	0.297950
	3	1.471	1298.305	19.118	18.395	0.350046
	4	1.549	1439.641	18.395	17.47	0.413769
Z20-2	1	1.587	1511.141	27.383	20.472	0.441069
	2	1.587	1511.141	20.472	19.926	0.470485
	3	1.587	1511.141	19.926	19.332	0.501585
	4	1.587	1511.141	19.332	19.09	0.513985

modal frequency can be used as the basis for evaluating the damage of the pier.

3.3. Comparative Analysis of the Pier Crack and Modal Frequency Damage. After the cumulative impact, the final damage degree of the high damage area (the bottom area of the pier and the vicinity of the impact point) of each pier is shown in Table 7.

The left and the right side areas in the table are the areas below the side of the impact point. It can be seen that the horizontal bending cracks appear in the front bottom region of each member and that the crack pattern and failure mode are the same. These cracks are similar in nature to typical curved cracks. The number, length, and maximum width of the main cracks in each area are shown in Table 8.

It can be seen from Table 8 that the development of pier crack width is consistent with the change of damage factor proposed by the pier modal frequency, and thus, it is feasible to identify the impact damage of reinforced concrete pier by modal frequency, and the modal frequency of the pier can be used to evaluate the damage degree.

4. Feasibility Analysis of Identification of Pier Damage by Ultrasonic Wave Velocity Verification Mode Frequency

4.1. Theoretical Analysis of the Relationship between the Pier Modal Frequency and the Ultrasonic Wave Velocity. For the identification of the impact damages of the reinforced concrete piers, this study mainly used the modal frequencies to identify and evaluate the test results, followed by a traditional ultrasonic detection method to verify the findings. In the ship-bridge collision simulations, the key variation following the pier damages was the elastic modulus E. It is known that if the stiffness K satisfies the first-order function relationship with the elastic modulus E as follows [32]:

$$K = f(E). \tag{3}$$

Then it can be known from the structural dynamics that

$$K = m\omega^2, \tag{4}$$

where m is the mass of the pier specimen (kg) and ω is the natural vibration frequency (Hz) of the pier specimen.

During the process of using the ultrasonic instruments to measure the damages, the function relationship between the wave velocity and elastic modulus in solid medium conformed to the following formula:

$$E = \rho V^2, \tag{5}$$

where ρ is the density of the concrete material (kg/m^3) and V is the ultrasonic wave velocity.

Then, in accordance with the relational expression shown above, the natural frequency ω of the bridge pier satisfied the first-order function relationship with the ultrasonic wave velocity V:

$$V = f(\omega). \tag{6}$$

Therefore, the relationship between the damage coefficients of the pier damages which had been identified by the modal frequencies and the damage coefficients of pier damages identified by ultrasonic wave velocities is the first-order function relationship which was found to be consistent. In other words, the modal frequencies and ultrasonic waves were consistent in this study's evaluation of the pier damages.

Table 7: Cracks in high damage area of the pier.

Specimen no.	Left side of impact point	Bottom area of impact point	Right side of impact point	Bottom back of impact point
Z16-1				
Z20-1				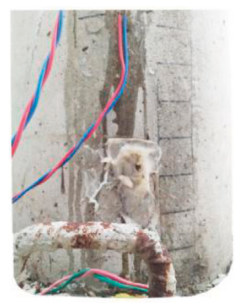
Z16-2		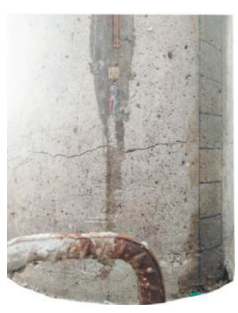		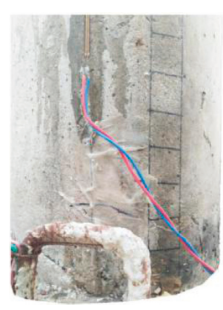
Z16-3				
Z20-2				

Table 8: Comparison of the numbers, lengths, and widths of the main cracks.

Specimen no.	Left side area			Bottom area of impact point			Right side area		
	Number	Length (mm)	Width (mm)	Number	Length (mm)	Width (mm)	Number	Length (mm)	Width (mm)
Z16-1	0	0	0	6	500	2.25	0	0	0
Z20-1	4	590	0.39	2	455	0.39	3	470	0.32
Z16-2	0	0	0	1	560	0.72	0	0	0
Z16-3	0	0	0	2	600	2.16	0	0	0
Z20-2	0	0	0	4	720	3.54	0	0	0

Table 9: Identification of the pier damages using the ultrasonic velocities of the test columns.

Specimen	Impact time	Impact velocity (m/s)	Impact energy (J)	Average acoustic velocity (m/s)		Damage factor D_2
				Before impact V_0	After impact V_b	
Z16-1	1	1.181	836.8566	4.796	4.577	0.089241
	2	1.376	1136.026	4.577	4.565	0.094010
	3	1.589	1514.953	4.565	4.471	0.130938
	4	1.717	1768.853	4.471	4.315	0.190525
Z20-1	1	1.047	657.7254	4.554	4.419	0.058410
	2	1.354	1099.99	4.419	4.355	0.085486
	3	1.603	1541.765	4.355	4.315	0.102208
	4	1.806	1956.982	4.315	4.104	0.187864
Z16-2	1	1.378	1139.33	4.369	4.181	0.084209
	2	1.336	1070.938	4.181	4.08	0.127920
	3	1.316	1039.114	4.08	3.886	0.208882
	4	1.316	1039.114	3.886	3.677	0.291690
Z16-3	1	1.496	1342.81	4.597	3.901	0.279883
	2	1.496	1342.81	3.901	3.888	0.284675
	3	1.471	1298.305	3.888	3.681	0.358816
	4	1.549	1439.641	3.681	3.542	0.406326
Z20-2	1	1.587	1511.141	4.449	3.802	0.269703
	2	1.587	1511.141	3.802	3.648	0.327666
	3	1.587	1511.141	3.648	3.596	0.346697
	4	1.587	1511.141	3.596	3.504	0.379698

4.2. Damage Analysis of Experimental Ultrasonic Wave Velocity. The ultrasonic detection of impact damages has a high sensitivity [33]. The damage criteria of concrete mainly include sound velocity, main frequency, and wave amplitude. Currently, many researchers have defined the damage variables of material through the changes in the wave velocities and have defined the damage factor D_2 as follows [34,35]:

$$D_2 = 1 - \frac{V_b^2}{V_0^2}, \tag{7}$$

where V_0 is the wave velocity before damage (m/s) and V_b is the wave velocity after damage (m/s).

The following table identifies the pier damages identified by the ultrasonic velocities of the test columns.

With the increase in the number of impacts, the damage factor of the pier gradually increases, which is a result of the change of the sound transmission medium. It can be seen from Table 9 that after each impact, the value of wave velocity gradually decreases and the change remains relatively stable, and thus, it can be used to judge the damage condition of the concrete after impact.

4.3. Comparative Analysis of Ultrasonic Damage and Modal Frequency Damage

4.3.1. Comparative Analysis. Figure 16 shows this study's comparisons of the fitting curves for the modal frequency damage factors and ultrasonic velocity damage factors of each test column under the conditions of equal impact velocity or accumulated impact energy. It can be seen from the figure that the damage factors of the modal frequencies and those of the ultrasonic velocities displayed a first-order relationship with the impact velocities. The two specimens had similar curve slopes, which indicated that the development and extensions of the pier damages were consistent under the two evaluation criteria and that the definition of the damage factors proposed in this study was feasible. Therefore, it was feasible to identify the pier impact damages using the modal frequencies.

4.3.2. D_1 and D_2 Fitting Curves. Figure 17 details the fitting curves of the correlation between the modal frequency damage factors and the ultrasonic velocity damage factors. Table 10 shows the analysis report for the fitting parameters

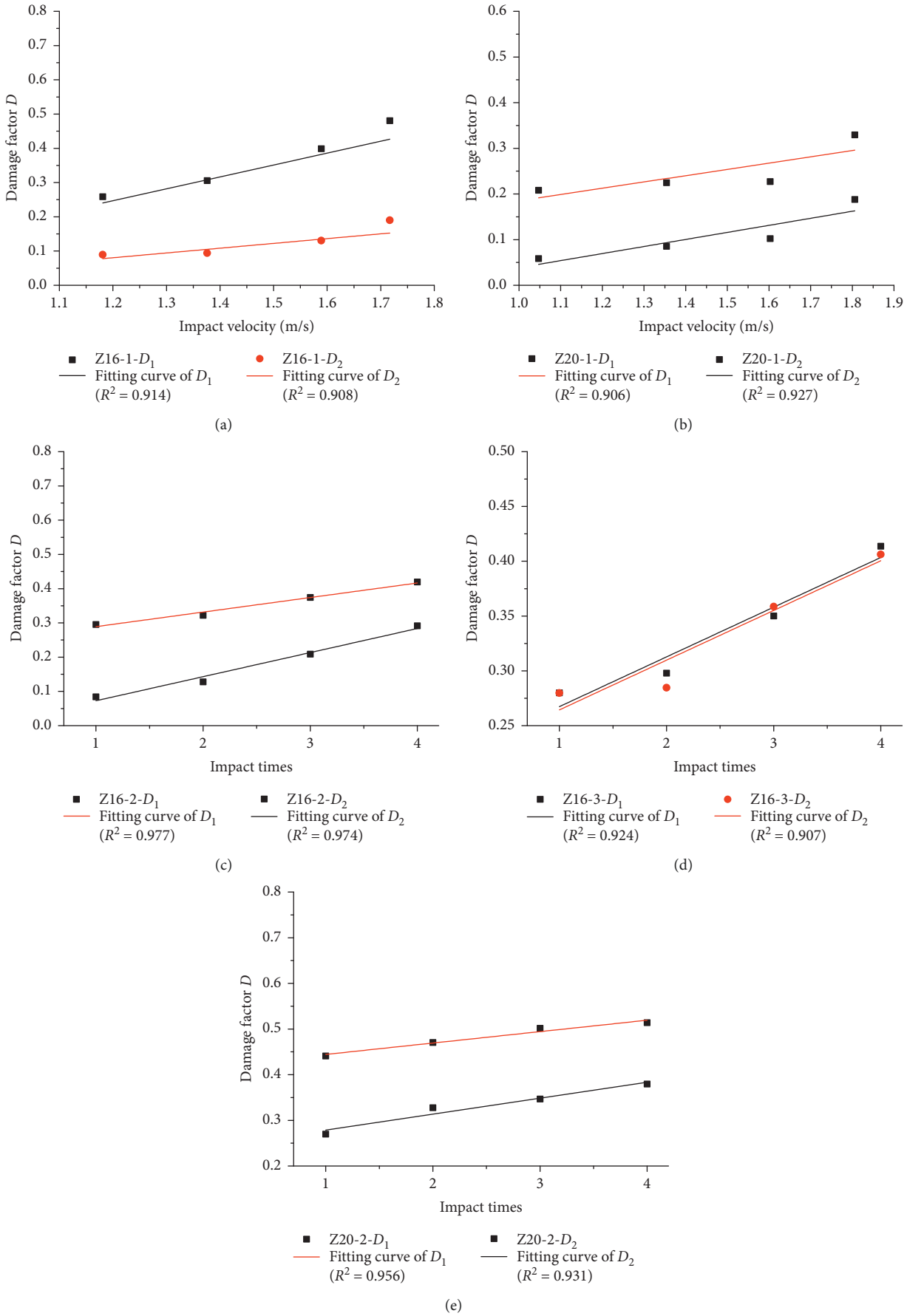

Figure 16: Comparative fitting curves for the modal frequency damage factors and ultrasonic velocity damage factors. (a) Comparative fitting curve of Z16-1, (b) comparative fitting curve of Z20-1, (c) comparative fitting curve of Z16-2, (d) comparative fitting curve of Z16-3, and (e) comparative fitting curve of Z20-2.

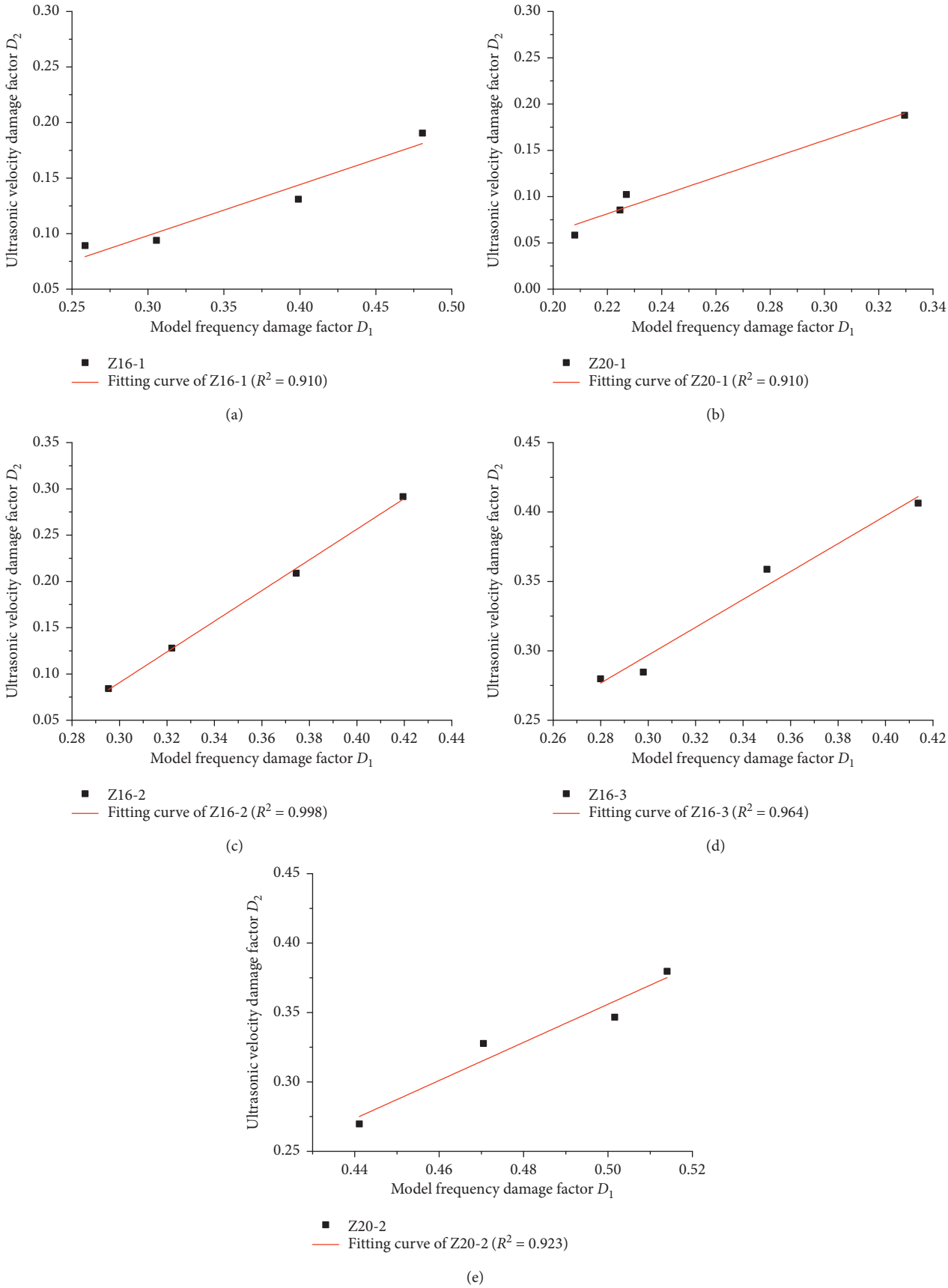

Figure 17: Fitting curves of the modal frequency damage factors and the ultrasonic velocity damage factors. (a) Fitting curve of Z16-1, (b) fitting curve of Z20-1, (c) fitting curve of Z16-2, (d) fitting curve of Z16-3, and (e) fitting curve of Z20-2.

Table 10: Analysis report for the fitting parameters of the fitting curves.

Specimen number	Intercept		Slope		Statistics Adj. R-square
	Value	Standard error	Value	Standard error	
Z16-1	−0.03939	0.03046	0.45869	0.0821	0.910
Z20-1	−0.13641	0.03311	0.99044	0.13143	0.910
Z16-2	−0.40649	0.01626	1.65719	0.04566	0.998
Z16-3	−0.00437	0.03806	1.00409	0.11212	0.964
Z20-2	−0.33039	0.10927	1.37269	0.22641	0.923

of the fitting curves. As can be seen in Figure 17, the modal frequency damage factors and the ultrasonic velocity damage factors showed a linear relationship. In other words, a first-order function relationship was observed, which confirmed that the modal frequencies and ultrasonic waves were consistent in characterizing the damages of the piers. It can be seen from Table 8 that the fitting goodness R^2 of each fitting curve was greater than 0.9. Also, the errors of the fitting values were within the allowable range, which indicated that the fitting degree was better in this test. The empirical formulas of the modal frequency damage factors and ultrasonic velocity damage factors could be roughly obtained as follows:

$$D_2 = \mu D_1 + \lambda, \tag{8}$$

where $\mu \in (0.45869, 1.65719), \lambda \in (-0.40649, -0.00437)$.

5. Conclusions

In order to explore the feasibility of the identification of pier impact damages using modal frequencies, horizontal impact tests were carried out on five reinforced pier specimens in this study. The relationships between the modal frequencies and ultrasonic velocities in characterizing and evaluating the pier impact damage were examined. The main conclusions which were reached in this study were as follows:

(1) The modal frequencies and ultrasonic waves had displayed consistency in the characterization and evaluations of the pier damages

(2) This study proposed that it was feasible to define the damage factors for identifying pier impact damages using a modal frequency method

(3) An empirical formula for the damage factors of the modal frequencies and ultrasonic velocities was obtained as follows: $D_2 = \mu D_1 + \lambda$, where $\mu\varepsilon 0.45869, 1.65719, \lambda\varepsilon(-0.40649, -0.00437)$

(4) Based on the abovementioned conclusions, it can be considered that it is feasible to identify and evaluate the impact damages of bridge piers using modal frequencies

6. Discussion

This research study concluded that the first-order function relationship between the damage factors of modal frequencies and the damage factors of the ultrasonic velocities could be written as follows: $D_2 = \mu D_1 + \lambda$, where $\mu\varepsilon 0.45869, 1.65719$ and $\lambda\varepsilon(-0.40649, -0.00437)$. The scopes of the parameters μ and λ were given according to the results of this study's experimental tests. It was impossible to give the determined values of μ and λ due to the limited test conditions. A large number of repeated tests would be required in order to obtain the accurate values. Therefore, in accordance with the deductions of the author, μ would approach 1 and λ would approach 0 after a large number of repeated tests were completed.

Data Availability

We verify that all our test data are accurate and reliable. The test data are included within the article and can be made freely available.

Conflicts of Interest

The authors declare that there are no conflicts of interest regarding the publication of this paper.

Acknowledgments

The research described in this paper was sponsored by the Major Project (Natural Science) of Department of Education of Guangdong Province (2014KZDXM064), the Science and Technology Innovation Project of Department of Education of Guangdong Province (2013KJCX0188), and the Civil Engineering Technology Research Center of Guangdong Province.

References

[1] Y. Ding and A. Li, "Structural health monitoring of long-span suspension bridges using wavelet packet analysis," *Earthquake Engineering and Engineering Vibration*, vol. 6, no. 3, pp. 289–294, 2007.

[2] G. Gholipour, C. Zhang, W.-H. Kang, and A. A. Mousavi, "Reliability analysis of girder bridge piers subjected to barge collisions," *Structure and Infrastructure Engineering*, vol. 15, no. 9, pp. 1200–1220, 2019.

[3] Q. Sun and H. Tang, "Numerical simulation of gravity type pier and ship oblique collision," *Journal of Chongqing University of Technology (Natural Science)*, vol. 32, no. 7, pp. 67–71, 2018.

[4] X. Zhang, C. Zhang, and Z. Duan, "Numerical simulation on impact responses and failure modes of steel frame structural columns subject to blast loads," *Journal of Shenyang Jianzhu University (Natural Science)*, vol. 25, no. 4, pp. 656–662, 2009.

[5] W. Ming-Yue, M. Bing-Rong, L. I. Xu-Juan et al., "Damage identification of continuous beam based on rotation mode

and wavelet neural network," *Chinese Quarterly of Mechanics*, vol. 37, no. 4, pp. 684–691, 2016.

[6] B. Zhao, D. Lei, J. Fu, L. Yang, and W. Xu, "Experimental study on micro-damage identification in reinforced concrete beam with wavelet packet and DIC method," *Construction and Building Materials*, vol. 210, pp. 338–346, 2019.

[7] M. Sanayei and O. Onipede, "Damage assessment of structures using static test data," *AIAA Journal*, vol. 29, no. 7, pp. 1174–1179, 1991.

[8] Y.-B. Yang, W.-F. Chen, H.-W. Yu, and C. S. Chan, "Experimental study of a hand-drawn cart for measuring the bridge frequencies," *Engineering Structures*, vol. 57, pp. 222–231, 2013.

[9] S. Beskhyroun and T. Oshima, S. Mikami and Y. Miyamori, Assessment of vibration-based damage identification techniques using localized excitation source," *Journal of Civil Structural Health Monitoring*, vol. 3, no. 3, pp. 207–223, 2013.

[10] L. T. Stutz, I. C. S. S. Rangel, L. S. Rangel, R. A. P. Corrêa, and D. C. Knupp, "Structural damage identification built on a response surface model and the flexibility matrix," *Journal of Sound and Vibration*, vol. 434, pp. 284–297, 2018.

[11] P. Hajela and F. J. Soeiro, "Structural damage detection based on static and modal analysis," *AIAA Journal*, vol. 28, no. 6, pp. 1110–1115, 1990.

[12] C. R. Farrar and S. W. Doebling, "Lessons learned from applications of vibration based damage identification methods to large bridge structure," in *Proceedings of the Structural Health Monitoring: Current Status and Perspectives*, pp. 351–370, Stanford, CA, USA, September 1997.

[13] N. Tandon and A. Choudhury, "A review of vibration and acoustic measurement methods for the detection of defects in rolling element bearings," *Tribology International*, vol. 32, no. 8, pp. 469–480, 1999.

[14] S. Fan, S. Zhao, B. Qi, and Q. Kong, "Damage evaluation of concrete column under impact load using a piezoelectric-based EMI technique," *Sensors*, vol. 18, no. 5, p. 1591, 2018.

[15] D. Feng and M. Q. Feng, "Experimental validation of cost-effective vision-based structural health monitoring," *Mechanical Systems and Signal Processing*, vol. 88, pp. 199–211, 2017.

[16] Y. Guo, *Monitoring-Based Assessment of Bridges Subject to Ship collision*, The Hong Kong Polytechnic University, Hong Kong, China, 2010.

[17] S. E. van Manen and A. G. Frandsen, "Ship collision with bridges, review of accidents," in *Ship Collision Analysis*, pp. 3–12, Routledge, Abingdon, UK, 2017.

[18] X. Zhou, Y. Gao, G. Zhang, and S. Xu, "Mechanical properties of equal-strength stainless reinforced replacement piers under lateral impact loading," *Advances in Mechanical Engineering*, vol. 10, no. 6, Article ID 1687814018778635, 2018.

[19] G. Gholipour, C. Zhang, and A. A. Mousavi, "Analysis of girder bridge pier subjected to barge collision considering the superstructure interactions: the case study of a multiple-pier bridge system," *Structure & Infrastructure Engineering Maintenance Management Life-Cycle Design & Performance*, vol. 15, no. 3, pp. 392–412, 2019.

[20] G. Zhang, S. Xu, H. Xie, X. Zhou, and Y. Wang, "Behavior of stainless steel–reinforced concrete piers under lateral impact loading," *Advances in Mechanical Engineering*, vol. 9, no. 5, 2017.

[21] X. Zhou, Y. Gao, F. Huang, and G. Zhang, "A study on the collision force of reinforced concrete piers under cumulative ship collision," *Advances in Mechanical Engineering*, vol. 11, no. 3, 2019.

[22] G. Gholipour, C. Zhang, and A. A. Mousavi, "Nonlinear numerical analysis and progressive damage assessment of a cable-stayed bridge pier subjected to ship collision," *Marine Structures*, vol. 69, 2020.

[23] W.-X. Ren and G. De Roeck, "Structural damage identification using modal data I: simulation verification," *Journal of Structural Engineering*, vol. 128, no. 1, pp. 87–95, 2002.

[24] J. Zhan, H. Xia, and J. Yao, "An impact vibration test method for measuring natural frequencies of existing piers," *Journal of Beijing Jiaotong University*, vol. 29, no. 1, 2005.

[25] J. Zhan, L. X. I. A. He, and J. Yao, "Numerical study on structural damage detection of pier based on modal parameters," *China Safety Science Journal (CSSJ)*, vol. 3, no. 3, pp. 171–175, 2007.

[26] M. M. F. Yuen, "A numerical study of the eigenparameters of a damaged cantilever," *Journal of Sound and Vibration*, vol. 103, no. 3, pp. 301–310, 1985.

[27] A. K. Pandey, M. Biswas, and M. M. Samman, "Damage detection from changes in curvature mode shapes," *Journal of Sound and Vibration*, vol. 145, no. 2, pp. 321–332, 1991.

[28] D. You-Sheng, "Analysis of calculating method of the natural frequency of bridge pier supported by pile foundation," *Journal of Yueyang Normal University*, vol. 4, no. 3, pp. 82-83, 2002.

[29] Y. B. Yang and J. P. Yang, "State-of-the-art review on modal identification and damage detection of bridges by moving test vehicles," *International Journal of Structural Stability and Dynamics*, vol. 18, no. 2, 2018.

[30] L. Sun, Y. Zhou, and Z. Min, "Experimental study on the effect of temperature on modal frequencies of bridges," *International Journal of Structural Stability and Dynamics*, vol. 18, no. 12, 2018.

[31] L. Zhu and A. Malekjafarian, "On the use of ensemble empirical mode decomposition for the identification of bridge frequency from the responses measured in a passing vehicle," *Infrastructures*, vol. 4, no. 2, p. 32, 2019.

[32] K. Worden, *Nonlinearity in Structural Dynamics: Detection, Identification and Modelling*, CRC Press, Boca Raton, FL, USA, 2019.

[33] Y. Tian, T. Huang, J. Liu, R. Jin, and C. Zhang, "Damage detection and compressive behavior of concrete after impacting," *Journal of Building Structures*, vol. 35, pp. 58–64, 2014.

[34] CECS 21- 2000, *Technical Specifications for the Inspections of Concrete Defects by Ultrasonic Methods*, China Association for Engineering Construction Standardization, Beijing, China, 2000.

[35] H. Wang and Y. Song, "Ultrasonic pulses behavior in various-size concrete specimens under compression," *Journal-Dalian University of Technology*, vol. 47, no. 1, p. 90, 2007.